



Erneux, T., Gavrielides, A., Green, K., & Krauskopf, B. (2003).
External cavity modes of semiconductor lasers with phase-conjugate feedback. <https://doi.org/10.1103/PhysRevE.68.066205>

Early version, also known as pre-print

Link to published version (if available):
[10.1103/PhysRevE.68.066205](https://doi.org/10.1103/PhysRevE.68.066205)

[Link to publication record in Explore Bristol Research](#)
PDF-document

University of Bristol - Explore Bristol Research

General rights

This document is made available in accordance with publisher policies. Please cite only the published version using the reference above. Full terms of use are available:
<http://www.bristol.ac.uk/red/research-policy/pure/user-guides/ebr-terms/>

External cavity modes of semiconductor lasers with phase-conjugate feedback

Thomas Erneux

*Université Libre de Bruxelles, Optique Nonlinéaire Théorique,
Campus Plaine, C.P. 231, 1050 Bruxelles, Belgium*

Athanasios Gavrielides

*Nonlinear Optics Group, Air Force Research Laboratory,
3550 Aberdeen Ave. SE, Kirtland AFB, NM 87117-5776, USA*

Kirk Green

Department of Computer Science, KU Leuven, Celestijnenlaan 200A, 3001 Heverlee, Belgium

Bernd Krauskopf

Department of Engineering Mathematics, University of Bristol, Bristol BS8 1TR, UK

(Dated: July 8, 2003)

External cavity modes (ECMs) of a semiconductor laser with phase-conjugate feedback are defined as time-periodic pulsating intensity solutions exhibiting a frequency close to an integer multiple of the external cavity frequency. As the feedback rate progressively increases from zero, they sequentially appear as stable attractors in the bifurcation diagram. We construct a simple analytical approximation of these pulsating intensity solutions and determine their frequencies. We show that branches of ECMs are isolated. Finally, the validity of our approximation is tested by comparing numerical bifurcation diagrams obtained by simulation and continuation techniques with our analytical results.

PACS numbers: 05.45.Jn, 42.55.Px, 42.65.Hw, 42.65.Sf

I. INTRODUCTION

The response of a laser subject to optical feedback is a key problem for both applied and theoretical research [1–4]. A weak optical feedback from a distant surface modifies the laser frequencies suggesting new imaging techniques [5, 6]. For semiconductor lasers, a weak optical feedback generates undesired dynamical instabilities because the delay of the feedback is large compared to the photon lifetime [7–11]. Examples of such laser systems include the laser subject to conventional optical feedback (COF) from an external mirror [12, 13] and the laser with phase-conjugate feedback (PCF) from a phase-conjugating mirror [14, 15], which is considered here.

Phase conjugation is a process in which the light that is reflected back from the phase conjugator has not only its direction of propagation reversed but it is also wave-front inverted [16]. The most important application of phase conjugation is the correction of optical distortions. In particular, for a distortion that occurs between the source and the phase conjugator, the light passing through the distortion after reflection from the phase conjugator returns to its original undistorted state. Phase conjugation is used today extensively in lasers to eliminate phase distortions due to heating and stress effects in the laser medium. A second interest of phase conjugation is stability; that is, PCF is preferred over COF because the full external round trip phase vanishes and the PCF laser cannot lock to an external cavity frequency.

There are, however, two difficulties that have delayed systematic comparisons between experiments and the-

ory. First, PCF is more difficult to realize than COF. The most common way of making a phase conjugator is through a four-wave mixing process in which two pump waves are coupled with the incident wave through a third-order susceptibility to produce the conjugated return wave [3]. Second, earlier numerical simulations [15, 17, 20, 21] and linear stability analyses [14, 19, 22] revealed a rich variety of possible outputs but with little insight on simple bifurcation mechanisms. This has motivated the recent development of numerical continuation methods. In particular, the application of the Matlab package DDE-BIFTOOL [23] has revealed important features of both the COF and PCF lasers. For the COF laser, branches emanating from Hopf bifurcations have been found connecting pairs of external cavity modes (so-called bridges) [24–28]. For the PCF laser, a sequence of isolated branches of pulsating intensity solutions exhibiting simple properties has been found [29]. Their apparent simplicity encourages analytical investigation. An asymptotic method that took advantage of the natural values of the laser parameters has been used in order to construct the bifurcation bridges in the COF laser [30]. In this paper, we use the same technique and construct an approximation of the PCF time-periodic intensity solutions found in Ref. [29].

As the feedback rate is progressively increased from zero, stable branches of pulsating intensity solutions sequentially appear between domains of chaotic dynamics [21]. Due to the fact that the intensity oscillates at a frequency close to an integer multiple of the external cavity frequency, these stable regimes have been called

external cavity modes (ECMs) by analogy to the ECMs of the COF laser [31]. Our analytical approximation of the ECMs of the PCF laser show that they sequentially appear as isolated branches in the bifurcation diagram and that they exhibit the expected frequencies. A large part of this paper is devoted to a comparison between analytical and numerical bifurcation diagrams.

The paper is organized as follows. In Section II we formulate the PCF laser equations in their dimensionless form and determine approximations to the Hopf bifurcation points. These approximations are based on specific scalings of the parameters and reveal two classes of Hopf bifurcation points. The first class of Hopf points appear at low feedback rates and exhibit a frequency close to the relaxation oscillation frequency of the solitary laser. The second class of Hopf points appear for much higher values of the feedback rate and their frequencies are proportional to the external cavity frequency. In Section III we determine the ECM pulsating intensity solutions by constructing an asymptotic solution. In Section IV we investigate their relationship with the Hopf bifurcation points found in Section II. The validity of our approximation is systematically investigated in Section V where numerical bifurcation diagrams obtained by simulation and continuation are compared with the analytical bifurcation diagrams. Finally, in Section VI we discuss the physical significance of our main results and review a series of open problems.

II. FORMULATION AND HOPF BIFURCATIONS

We consider rate equations for a semiconductor laser subject to instantaneous PCF in dimensionless form; this formulation is briefly described in Appendix A. For analytical simplicity, we neglect nonlinear gain saturation, an effect included in Refs. [21, 29, 32–34], and as is usual in the literature, set the phase and frequency shift at the PCM to zero. These simplifications are however not limitations of our analysis. The PCF equations for the complex electric field Y and the carrier density Z are then given by

$$Y' = (1 + i\alpha)ZY + \gamma Y^*(t - \theta), \quad (1)$$

$$TZ' = P - Z - (1 + 2Z)|Y|^2 \quad (2)$$

where prime denotes differentiation with respect to the dimensionless time t . In these equations, α is the linewidth enhancement factor, γ is the dimensionless feedback rate, $\theta = \tau/\tau_p$ is the external cavity round-trip time normalized by the photon lifetime, $T = \tau_e/\tau_p$ is defined as the ratio of the carrier and photon lifetimes, and P is the pump parameter above threshold. Using the values given in Refs. [21, 29, 32–34], we find

$$\alpha = 3, \theta = 476, T = 1429 \text{ and } P = 4.17 \times 10^{-2}. \quad (3)$$

Equations (1) and (2) have \mathbb{Z}_2 -symmetry in the transformation $(Y, Z) \rightarrow (-Y, Z)$. This means that any

| | $\gamma\theta$ | σ | C | $\sigma\theta$ | $C\theta$ |
|-------|----------------|----------------------|-----------------------|----------------|-----------|
| H_1 | 0.53 | 8.9×10^{-3} | -3.6×10^{-4} | 4.23 | -0.17 |
| H_2 | 0.63 | 7.1×10^{-3} | 4.2×10^{-4} | 3.38 | 0.20 |
| H_3 | 0.73 | 5.4×10^{-3} | -4.9×10^{-4} | 2.55 | -0.23 |
| | 9.50 | 1.7×10^{-2} | 6.5×10^{-3} | 7.95 | 3.00 |

TABLE I: Hopf bifurcations for low feedback rate and σ close to $\omega_R = 7.6 \times 10^{-3}$. The first three Hopf bifurcations points have been labelled in terms of increasing values of $\gamma\theta$. The last solution exhibits a large value of $\gamma\theta$ which contradicts our scaling assumptions (6). The approximated Hopf points have been labelled according to their relation with the numerical solutions shown in Table III.

solution will either be symmetric or have a symmetric counterpart obtained by a rotation by π of the Y -plane [35]. Apart from the trivial steady state solution, that is $(Y, Z) \equiv (0, P)$, there exist two distinct branches of nonsymmetric steady states given by (B5)–(B7) in Appendix B.

The conditions for a Hopf bifurcation are given by (B8) and (B9) where C and σ represent the amplitude of Z and the frequency of the oscillations at the Hopf bifurcation point, respectively. These equations are transcendental equations which are difficult to solve even numerically. Our analysis differs from previous attempts to solve the Hopf conditions [17, 22] by the application of asymptotic techniques [36, 37]. Specifically, we take advantage of the large value of T and look for an approximation for C and σ . To this end, we introduce a small parameter ε defined by

$$\varepsilon \equiv T^{-1} \quad (4)$$

with which we scale C and σ . We also need to specify the scalings of the other laser parameters since distinguished limits of the Hopf equations (B8)–(B9) are possible in the small ε limit.

The simplest approximation is based on the idea that for low feedback rates, the frequency at the Hopf bifurcation must be close to the laser relaxation frequency defined in Ref. [38] as

$$\omega_R \equiv (2\varepsilon P)^{1/2}. \quad (5)$$

Assuming the scalings

$$\begin{aligned} P &= O(1), \quad C = O(\varepsilon), \quad \theta = O(\varepsilon^{-1}) \quad \text{and} \\ \sigma &= O(\varepsilon^{1/2}), \end{aligned} \quad (6)$$

we collect the leading terms in (B8) and (B9). We find

$$\sigma^3 + 2\varepsilon P [-(1 + \alpha^2)C \sin(\sigma\theta) - \sigma] = 0, \quad (7)$$

$$\begin{aligned} -2\sigma^2 C &+ \varepsilon(1 + 2P)\sigma^2 \\ &+ 2\varepsilon P(1 + \alpha^2)C(\cos(\sigma\theta) + 1) = 0 \end{aligned} \quad (8)$$

| | $\gamma\theta$ | $\sigma\theta$ | $C\theta$ ($\varepsilon = 0$) | $C\theta$ ($\varepsilon \neq 0$) |
|-------|----------------|----------------|---------------------------------|------------------------------------|
| H_4 | 5.84 | 7.39 | 1.85 | 1.20 |
| H_5 | 6.58 | 8.32 | -2.08 | -2.02 |
| H_6 | 9.06 | 11.46 | -2.87 | -2.13 |
| H_7 | 8.33 | 10.53 | 2.63 | 2.66 |

TABLE II: Hopf bifurcation points for $\sigma\theta = O(1)$, $\varepsilon = 0$ (column $C\theta$ ($\varepsilon = 0$)) and $\varepsilon\theta^2 = O(1)$ (column $C\theta$ ($\varepsilon \neq 0$)). The latter values were computed with an improved approximation and they are much closer to the respective numerical solutions shown in Table III.

where all neglected terms are of order $O(\varepsilon^{5/2})$ or smaller. Using (8), we determine C as

$$C = \frac{\varepsilon(1 + 2P)\sigma^2}{2\sigma^2 - 2\varepsilon P(1 + \alpha^2)(\cos(\sigma\theta) + 1)}. \quad (9)$$

Inserting (9) into (7), we obtain the following equation for σ only

$$F(\sigma) \equiv \sigma^2 - 2\varepsilon P - 2\varepsilon P(1 + \alpha^2) \cdot \frac{\varepsilon(1 + 2P)\sigma \sin(\sigma\theta)}{2\sigma^2 - 2\varepsilon P(1 + \alpha^2)(\cos(\sigma\theta) + 1)} = 0. \quad (10)$$

This equation resembles the equation for the Hopf frequency of the COF laser (see (19) in Ref. [38]) except that in the denominator of the last term, there is an extra $2\sigma^2$ contribution and $\cos(\sigma\theta) + 1$ replaces $\cos(\sigma\theta) - 1$. We use the values of the parameters (3) and solve (10) for σ . We then determine $C\theta$ from (9) and $\gamma\theta = \sqrt{1 + \alpha^2}|C|\theta$ comes from the steady state relations (B5) and (B6). A graphical study of the function $F(\sigma)$ as a function of σ indicates four roots. They are listed in Table I.

The approximations of the first three Hopf bifurcations shown in Table I are in excellent agreement with the values obtained by continuation using DDE-BIFTOOL; see already Table III. An analysis of the real eigenvalues of the characteristic equation indicates that the steady state with $C > 0$ is always unstable, namely a saddle. Thus, only the Hopf bifurcation with $C < 0$ may lead to stable oscillations. The first three solutions satisfy $\gamma\theta < 1$ and agree with our assumption that γ is a small $O(\varepsilon)$ quantity. The last solution in Table I corresponds to a large value of γ and is not a valid approximation. However, it suggests that there exist other Hopf bifurcations that satisfy different scaling laws.

We may obtain a different approximation of the Hopf bifurcation for $\gamma\theta = O(1)$ if we consider the case

$$P = O(1), C\theta = O(1) \text{ and } \sigma\theta = O(1) \quad (11)$$

as $\varepsilon \rightarrow 0$. Neglecting all ε terms in (B8) and (B9), the Hopf bifurcation conditions then reduce to

$$(1 + \alpha^2)C^2(\cos(2\sigma\theta) - 1) + \sigma^2 = 0, \quad (12)$$

$$(1 + \alpha^2)C \sin(2\sigma\theta) - 2\sigma = 0. \quad (13)$$

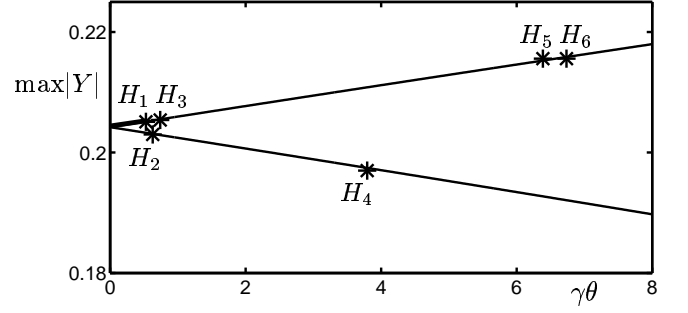


FIG. 1: Analytical bifurcation diagram of the two steady state branches. The upper branch is stable until the first Hopf bifurcation H_1 . The lower branch is always unstable. Other Hopf bifurcation points have been determined analytically and are shown in the figure. At these Hopf bifurcations, nearly vertical Hopf branches appear and connect steady state and ECMs branches; compare Fig. 4. The bifurcation details of these connections are not revealed by the leading order bifurcation equations.

From (13), we extract C as

$$C = \frac{2\sigma}{(1 + \alpha^2) \sin(2\sigma\theta)}. \quad (14)$$

Inserting (14) into (12), we obtain an equation for σ only. The solutions with $\sigma \neq 0$ satisfy the condition

$$\cos(\sigma\theta) = \pm \sqrt{\frac{2}{1 + \alpha^2}}. \quad (15)$$

We determine $\sigma\theta$ from (15), obtain $C\theta$ from (14) and compute $\gamma\theta = \sqrt{1 + \alpha^2}|C|\theta$. Solutions with $1.5 < |C\theta| < 3$ are listed in Table II in the column $C\theta$ ($\varepsilon = 0$).

Comparing these results with the numerical solutions listed in Table III, the agreement is good for H_5 but not for the other points. In order to improve our approximations, we need to take into account the relatively large value of θ . From the Hopf conditions (B8) and (B9), we note that the neglected terms are proportional to $\varepsilon\theta$ and $\varepsilon\theta^2$ which are numerically significant. We may take into account the effect of ε by investigating the double limit $\varepsilon \rightarrow 0$, $\theta \rightarrow \infty$ but keeping

$$\varepsilon\theta^2 = O(1) \quad (16)$$

fixed. With (11) and (16), (B8) and (B9) now reduce to

$$0 = \sigma [(1 + \alpha^2)C^2(\cos(2\sigma\theta) - 1) + \sigma^2] - 2\varepsilon P [(1 + \alpha^2)C \sin(\sigma\theta) + \sigma], \quad (17)$$

$$0 = \sigma [(1 + \alpha^2)C \sin(2\sigma\theta) - 2\sigma] + 2\varepsilon P(1 + \alpha^2)(\cos(\sigma\theta) + 1). \quad (18)$$

The solution of these equations for $C\theta$ and ε can be found analytically in parametric form. We determine C from

(18) and insert its expression into (17). This results in a quadratic equation for ε which we solve in terms of σ . Having $\varepsilon = \varepsilon(\sigma)$, we determine $C = C(\sigma)$. In Table II, the new values for $C\theta$ (in the column for $\varepsilon \neq 0$) are compared to their earlier estimates obtained with $\varepsilon = 0$.

In Fig. 1 we plot the steady state branches, which are determined from (B5)–(B7), together with the Hopf bifurcation points from Table I and Table II. The lower branch is always unstable and the upper branch is stable until the first Hopf bifurcation H_1 . The relevance of the Hopf bifurcation points for the ECM intensity solutions is discussed in Section IV.

III. EXTERNAL CAVITY MODES

We next concentrate on the pulsating intensity solutions described in Ref. [29]. These solutions are characterized by oscillating frequencies that are comparable to the external cavity frequency. This suggests to seek a solution that depends on the basic time t . We take advantage of the large value of T and seek a solution of (1) and (2) of the form

$$Y = Y_0(t) + \varepsilon Y_1(t) + \dots \quad (19)$$

$$Z = Z_0(t) + \varepsilon Z_1(t) + \dots \quad (20)$$

where ε is defined by (4). Introducing (19) and (20) into (1) and (2) and equating to zero the coefficients of each power of ε leads to a sequence of linear problems to solve. The equations for Y_0 , Z_0 and Z_1 are given by

$$Y_0' = (1 + i\alpha)Z_0Y_0 + \gamma Y_0^*(t - \theta), \quad (21)$$

$$Z_0' = 0, \quad (22)$$

$$Z_1' = P - Z_0 - (1 + 2Z_0)|Y_0|^2. \quad (23)$$

Equation (22) implies that

$$Z_0 = C \quad (24)$$

is a unknown constant. Equation (21) is then linear and admits a solution of the form

$$Y_0 = A_1 \exp(i\omega t) + A_2 \exp(-i\omega t) \quad (25)$$

provided that A_1, A_2 satisfy the following homogeneous system of equations

$$[-i\omega + (1 + i\alpha)C] A_1 + \gamma A_2^* \exp(-i\omega\theta) = 0, \quad (26)$$

$$\gamma A_1^* \exp(i\omega\theta) + [i\omega + (1 + i\alpha)C] A_2 = 0. \quad (27)$$

These equations have a nontrivial solution if ω and C satisfy the characteristic equation

$$[-i\omega + (1 + i\alpha)C] [-i\omega + (1 - i\alpha)C] - \gamma^2 \exp(-2i\omega\theta) = 0. \quad (28)$$

From the real and imaginary parts of (28), we find

$$-\omega^2 + (1 + \alpha^2)C^2 - \gamma^2 \cos(2\omega\theta) = 0, \quad (29)$$

$$-2\omega C + \gamma^2 \sin(2\omega\theta) = 0. \quad (30)$$

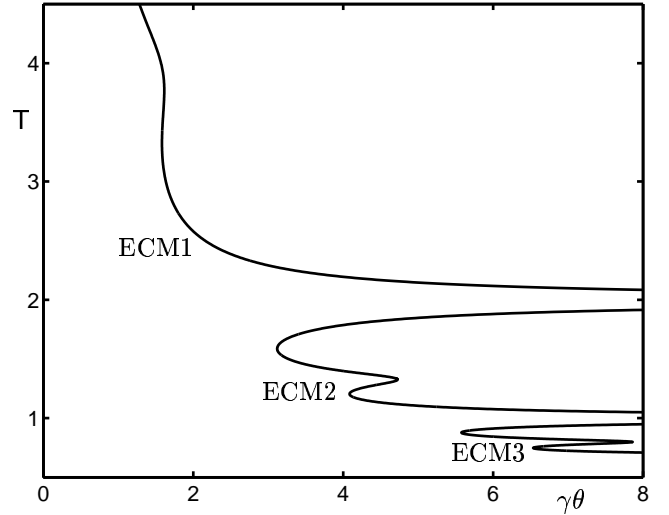


FIG. 2: Analytical bifurcation diagram of the first three ECMs. The figure represents the period $T = 2\pi/\omega$ of $Y(t)$ as a function of $\gamma\theta$. The frequency ω is determined from (32). Comparing with the numerical solutions obtained by DDE-BIFTOOL in Fig. 5, a lower part of each isolated branch corresponds to a stable ECM.

Using (30), we have

$$C = \frac{\gamma^2 \sin(2\omega\theta)}{2\omega}, \quad (31)$$

and inserting (31) into (29), we obtain the following equation for ω only

$$-\omega^2 + \frac{\gamma^4 \sin^2(2\omega\theta)}{4\omega^2} (1 + \alpha^2) = \gamma^2 \cos(2\omega\theta). \quad (32)$$

Equation (32) is a quadratic equation for $\gamma^2 = \gamma^2(\omega)$ which can be solved. Figure 2 represents the period $T \equiv 2\pi/\omega$ as a function of $\gamma\theta$. The three Σ -shaped branches are similar to the branches shown in Figure 4 in Ref. [29], and verified later in Section V, where it is shown that the lower part of each pulsating intensity branch may exhibit stable solutions. The lower branches are close to their asymptotic values as $\gamma\theta \rightarrow \infty$; that is,

$$T\theta^{-1} = 2/n \quad (33)$$

where $n = 1, 2, \dots$. Using (25), we compute the intensity of the laser field as

$$|Y|^2 \simeq |A_1|^2 + |A_2|^2 + 2|A_1||A_2|\cos(2\omega t + \psi) \quad (34)$$

where ψ is a constant phase. The intensity exhibits harmonic oscillations with a period equal to π/ω or $T/2$.

The leading solution (25) is not completely determined. Equation (26) (or (27)) provides a first relationship between A_1 and A_2 . To find a second relationship between A_1 and A_2 , we apply a solvability condition for

(23). Indeed, the condition for a bounded Z_1 requires that

$$P - C - (1 + 2C)(|A_1|^2 + |A_2|^2) = 0. \quad (35)$$

Using (27), $|A_2|^2$ is given by

$$|A_2|^2 = \frac{\gamma^2}{C^2 + (\omega + C\alpha)^2} |A_1|^2, \quad (36)$$

which, by inserting into (35), gives $|A_1|^2$ as

$$|A_1|^2 = \left(\frac{P - C}{1 + 2C} \right) \left(\frac{C^2 + (\omega + C\alpha)^2}{C^2 + (\omega + C\alpha)^2 + \gamma^2} \right). \quad (37)$$

Knowing $|A_1|$ and $|A_2|$, we determine the intensity from (34). The π/ω -periodic intensity oscillates with extrema given by $|Y|^2 = (|A_1| \pm |A_2|)^2$.

IV. HOPF BIFURCATION BRANCHES

Our previous analysis of the ECM solutions need to be revised near particular points where the ECM solution and the steady state solution admits the same value of C (same carrier number $Z_0 = C$). At and near these points, we have a solution of (21) of the form

$$Y_0 = A_0 + A_1 \exp(i\omega t) + A_2 \exp(-i\omega t) \quad (38)$$

where A_0 , A_1 , and A_2 are three unknowns. Substituting (38) into (21), we find that such a solution is possible provided that the three amplitudes satisfy both the steady state equation and the pulsating intensity solution equations. They are given by

$$-C(1 + i\alpha)A_0 = \gamma A_0^*, \quad (39)$$

$$i\omega A_1 - C(1 + i\alpha)A_1 = \gamma A_2^* \exp(-i\omega\theta), \quad (40)$$

$$-i\omega A_2 - C(1 + i\alpha)A_2 = \gamma A_1^* \exp(i\omega\theta). \quad (41)$$

From (39)–(41), we find that a solution with all three amplitudes differing from zero is possible provided C , γ and ω satisfy the conditions

$$C = \pm \frac{\gamma}{\sqrt{1 + \alpha^2}} = \frac{\gamma^2 \sin(2\omega\theta)}{2\omega}, \quad (42)$$

$$-\omega^2 + \frac{\gamma^4 \sin^2(2\omega\theta)}{4\omega^2} (1 + \alpha^2) = \gamma^2 \cos(2\omega\theta). \quad (43)$$

Equations (42) and (43) lead to critical values for γ and ω . Using (42), we first determine γ as

$$\gamma = \pm \frac{2\omega}{\sqrt{1 + \alpha^2} \sin(2\omega\theta)} > 0 \quad (44)$$

and by substituting (44) into (43), we obtain a simple equation for ω given by

$$\cos(\omega\theta) = \pm \sqrt{\frac{2}{1 + \alpha^2}}. \quad (45)$$

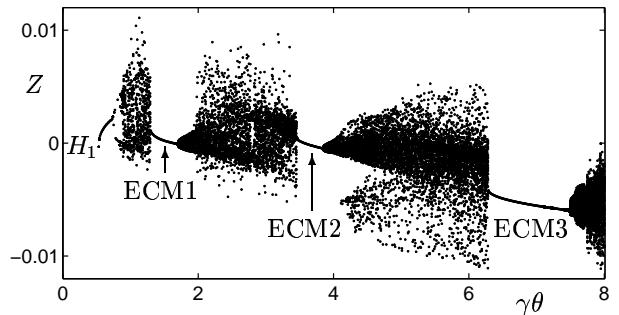


FIG. 3: Numerical bifurcation diagram of the stable attractors obtained by simulation. The figure shows the value of $Z(t)$ whenever the intensity $|Y(t)|^2$ crosses its average value in the increasing direction as a function of $\gamma\theta$.

Equations (44) and (45) are identical to the Hopf bifurcation conditions (14) and (15) if we replace ω by σ and γ by $|C| \sqrt{1 + \alpha^2}$. Note that $|A_1| = |A_2| = 0$ at the steady state branches where $|A_0| \neq 0$, and that $|A_0| = 0$ at the ECM solution branches where $|A_1| \neq 0$ and $|A_2| \neq 0$. All three amplitudes are not completely determined by the leading order equations (39)–(41) and require a higher order analysis which will not be presented here. We have found that the Hopf bifurcation branches are vertical as $\varepsilon \rightarrow 0$ and they provide a plausible connection between steady and ECM branches. Figure 4 shows the bifurcation diagram of the steady states obtained numerically by continuation, and it exhibits nearly vertical bifurcations. Figure 5 shows the Hopf bifurcation branch emerging from H_1 , which connects to the second ECM branch.

V. NUMERICAL BIFURCATION DIAGRAMS

In this section we investigate the bifurcation diagram of the stable solutions of the PCF equations. We first consider the parameters listed in (3); that is, the values used in Refs. [21, 29, 32–34] without nonlinear gain saturation. Figure 3 shows that, as the feedback rate $\gamma\theta$ progressively increases from zero, the stable steady state undergoes a Hopf bifurcation H_1 at $\gamma\theta \approx 0.53$ leading to stable periodic oscillations exhibiting a frequency close to the laser relaxation oscillation frequency (5). The stable periodic solution then undergoes a period-doubling bifurcation at $\gamma\theta \approx 0.73$, the first of a period-doubling cascade to a domain of more complex, chaotic dynamics. At $\gamma\theta \approx 1.29$ we observe that the laser locks into the first ECM solution with an intensity oscillating at a frequency close to $2\pi\theta^{-1}$. This agrees with our analysis indicating that the first ECM branch admits a period close to $T\theta^{-1} = 2\pi(\omega\theta)^{-1} = 2$. This implies $\omega = \pi\theta^{-1}$ and since the frequency of the intensity equals 2ω , we find $2\pi\theta^{-1}$. The first branch of ECM solutions is stable until $\gamma\theta \approx 1.67$ where it undergoes a torus bifurcation leading

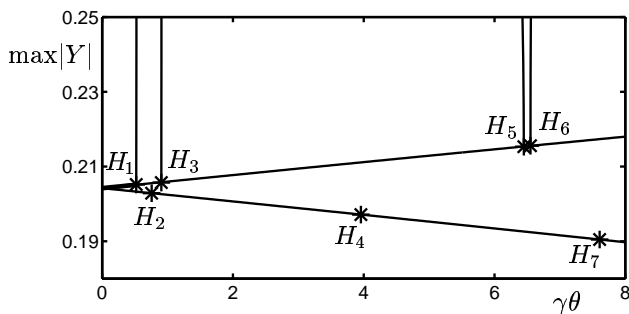


FIG. 4: Numerical bifurcation diagram of the steady state solutions obtained by continuation; compare Fig. 1. The figure shows the maximum of $|Y|$ as a function of $\gamma\theta$. Stable (unstable) steady state solutions are drawn by thick (thin) lines. Hopf bifurcation points are shown by stars. Also shown are the branches of periodic solutions emanating from the Hopf bifurcation points located on the upper steady state branch. They are nearly vertical as anticipated by the analysis.

to a new domain of chaotic dynamics. This torus bifurcation and the subsequent route to chaos in the PCF laser with nonlinear gain was detailed in Ref. [33]. The chaotic dynamics ends in a sudden transition to the second ECM solution at $\gamma\theta \approx 3.46$. Again, this branch of stable solutions undergoes a torus bifurcation at $\gamma\theta \approx 3.82$ leading to a third domain of chaotic dynamics. The third stable ECM appears at $\gamma\theta \approx 6.28$ and is destabilised in another torus bifurcation at $\gamma\theta \approx 7.39$ leading to a fourth and final domain of chaotic dynamics in our $\gamma\theta$ -range of consideration.

In the next section, we investigate the steady state and periodic solutions of the PCF laser using the continuation package DDE-BIFTOOL [23]. This approach has the advantage that one is able to compute solutions irrespective of their stability. Furthermore, as well as providing stability information of solutions, the position and the frequency of the Hopf bifurcation points can be obtained.

A. Steady states

Figure 4 shows a bifurcation diagram obtained by continuation with DDE-BIFTOOL. Stable solutions are drawn as a thick line, unstable solutions by a thin line. Two branches of steady state solutions are seen to be born at the onset of feedback. The upper branch is initially stable. It is destabilised in a Hopf bifurcation H_1 at $\gamma\theta \approx 0.522$, agreeing with the value obtained by simulation; see Figure 3. The ensuing branch of unstable steady state solutions undergo further Hopf bifurcations H_3 , H_5 and H_6 at $\gamma\theta \approx 0.906$, 6.449 and 6.550 , respectively. The lower branch is always unstable. It is seen to undergo Hopf bifurcations H_2 , H_4 and H_7 at $\gamma\theta \approx 0.756$, 3.942 and 7.624 , respectively. References [32] and [34]

| | $\gamma\theta$ | $\sigma\theta$ | $C\theta_{\text{num}}$ | $C\theta_{\text{anal}}$ |
|-------|----------------|----------------|------------------------|-------------------------|
| H_1 | 0.522 | 4.318 | -0.165 | -0.17 |
| H_2 | 0.756 | 3.337 | 0.239 | 0.20 |
| H_3 | 0.906 | 2.647 | -0.287 | -0.23 |
| H_4 | 3.942 | 7.883 | 1.247 | 1.20 |
| H_5 | 6.449 | 7.648 | -2.039 | -2.02 |
| H_6 | 6.550 | 11.18 | -2.071 | -2.13 |
| H_7 | 7.624 | 5.474 | 2.411 | 2.66 |

TABLE III: Values of the bifurcation parameter $\gamma\theta$, frequency $\sigma\theta$, and steady state value of the carrier density $C\theta$ at the Hopf bifurcation points H_1 to H_7 . All values were calculated using DDE-BIFTOOL. The last column indicates the approximative values determined analytically (repeated from Tables I and II).

contain detailed continuation studies of this steady state solution.

Table III contains further information, obtained with DDE-BIFTOOL, on the frequency σ and the amplitude of $Z \equiv C$ at the Hopf bifurcation points. These values agree well with the analytical estimates listed in Table I and Table II. The first three Hopf bifurcations are characterized by frequencies close to the relaxation oscillation frequency of the laser ($\omega_R\theta = 3.602$) and values of $\gamma\theta < 1$; see Table I. The next four Hopf bifurcations exhibit much larger values for γ and σ ($\gamma\theta > 1$); see Table II.

From the Hopf bifurcation points emanate branches of nonsymmetric periodic orbits. Symmetric periodic solutions exhibit a period $2\pi/\omega$ for the field Y and a period π/ω for the intensity $|Y|^2$. Nonsymmetric periodic solutions exhibit the same period $2\pi/\omega$ for both the field and the intensity [35]. The isolated branches of periodic intensity solutions determined analytically correspond to the branches of symmetric periodic solutions emerging at the limit points $\gamma\theta \approx 1.295$, $\gamma\theta \approx 3.733$ and $\gamma\theta \approx 6.283$, respectively; see Figure 5. These values are slightly lower than those documented analytically; see Figure 2. Figure 4 shows that the Hopf bifurcation branches are nearly vertical close to the Hopf points, again in agreement with the analytical results. In Ref. [29] it was shown that these branches connect the branches of pulsating intensity solutions. This is confirmed here, with some minor differences. Specifically, in Ref. [29], the first Hopf bifurcation branch was shown to connect to the first ECM, however, in the case presented here, that is without nonlinear gain, we find that the branch emerging from H_1 connects to the second ECM. The branch of periodic solutions emanating from H_3 does not connect to any ECMs. The branch emanating from H_5 connects to the third ECM branch, and the branch emanating from H_6 leaves our $\gamma\theta$ -range of consideration.

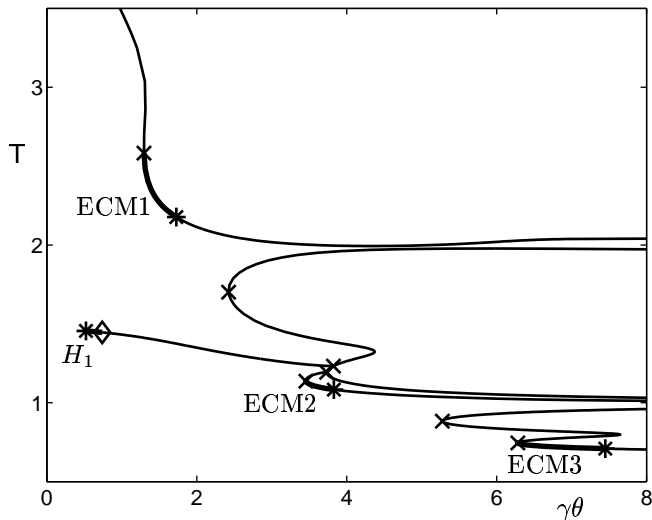


FIG. 5: Numerical bifurcation diagram of the first three ECMs obtained by continuation; compare Fig. 2. The figure represents the period T of $Y(t)$ as a function of $\gamma\theta$. The stable ECM solutions are drawn by thick lines. They are born at limit points in saddle-node bifurcations (\times) and destabilized in torus bifurcations ($*$). Also shown is the stable branch of periodic solutions emanating from the first Hopf bifurcation H_1 and destabilized in a period doubling bifurcation (\diamond).

B. Periodic solutions

Figure 5 shows three isolated branches of symmetric periodic solutions corresponding to the pulsating intensity solutions constructed analytically. They have been obtained with DDE-BIFTOOL. Also shown is the branch of nonsymmetric periodic solutions emanating from the Hopf bifurcation point H_1 and connecting to the second isolated branch of symmetric periodic solutions. The solutions are stable when drawn as a thick curve and unstable when drawn as a thin curve. The three isolated branches agree with the branches computed in Ref. [29] and are in very good agreement both in shape and position with the branches computed analytically and shown in Figure 2. They are born in saddle-node bifurcations of limit cycles at the limit points $\gamma\theta \approx 1.295$, $\gamma\theta \approx 3.733$ and $\gamma\theta \approx 6.283$, respectively. These values are slightly lower than those given analytically; compare with Figure 2. Finally, we note that the second stable ECM does not lie on the lower branch of the second isolated branch of symmetric periodic solutions but on a very close branch of nonsymmetric periodic solutions exhibiting a limit point at $\gamma\theta \approx 3.453$. This branch of solutions has not been found analytically.

| | analytical | simulation | continuation |
|---------|------------|------------|--------------|
| ECM_1 | 1.6 | 1.6 | 1.57 |
| ECM_2 | 4.0 | 4.2 | 4.08 |
| ECM_3 | 6.6 | 6.7 | 6.53 |

TABLE IV: Comparison between numerical and analytical estimates of the ECM limit points for $T = 3429$ and $\theta = 76$.

C. Comparison with analytical results

As we already discussed in Section II, the determination of the Hopf bifurcation points assuming $\gamma\theta = O(1)$ is valid provided $\varepsilon\theta^2$ is sufficiently small rather than ε small. By investigating the double limit of ε small and θ large, keeping $\varepsilon\theta^2$ fixed, we obtained a better estimation of the Hopf bifurcation points. In this section, we review the laser equations by introducing full scalings for all dependent and independent variables. From Section II we know that an ECM solution exhibits a frequency ω proportional to θ^{-1} , that Y is proportional to \sqrt{P} , and that $Z \approx C$ is proportional to θ^{-1} . This motivates introducing the new variables s , y and z defined by

$$s = t/\theta, Y = \sqrt{P}y \text{ and } Z = \theta^{-1}z. \quad (46)$$

From (1) and (2), we then obtain

$$y' = (1 + i\alpha)yz + \gamma\theta y^*(s - 1), \quad (47)$$

$$z' = \varepsilon_1 \left[1 - \theta^{-1}P^{-1}z - (1 + 2\theta^{-1}z)|y|^2 \right] \quad (48)$$

where the prime means differentiation with respect to the new time s , $\gamma\theta = O(1)$, and $\varepsilon = T^{-1}$ is now replaced by

$$\varepsilon_1 \equiv \theta^2 PT^{-1}. \quad (49)$$

The parameters (3) imply that $\varepsilon_1 \approx 7$, that is, ε_1 is large, which explains the relatively poor quantitative agreement between the analytical and the numerical bifurcation diagram. However, as the successive ECMs sequentially appear at larger values of $\gamma\theta$, the agreement will improve since rescaling s and z as $\bar{s} = \gamma\theta s$ and $z = \gamma\theta \bar{z}$ leads to

$$\varepsilon_2 = \varepsilon_1(\gamma\theta)^{-2} \quad (50)$$

as the coefficient multiplying the right-hand side of the \bar{z} equation. If $\gamma\theta = 10$, the small parameter is $\varepsilon_2 \approx 0.07$.

In order to quantitatively evaluate the validity of our asymptotic analysis, we consider the exaggerated value of $T = 3429$ and a smaller value of $\theta = 76$. We now find from (49) that $\varepsilon_1 \approx 0.07$, and this is sufficiently small for our analytical results. From numerical experiments not presented here, we note that the first Hopf bifurcation exhibits a frequency close to the relaxation oscillation frequency at $\gamma\theta \approx 0.04$ and is then followed by a burst of chaotic dynamics. At $\gamma\theta \approx 0.95$, the stable steady state reappears and undergoes a new Hopf bifurcation at $\gamma\theta \approx 1.55$. This bifurcation is quickly followed by

a small domain of complex oscillations that terminate as the laser locks to the first ECM. The same pattern then appears sequentially. In Table IV, we compare the numerical and analytical estimates for the limit points (saddle-node bifurcations of periodic orbits) where the three first pulsating intensity solutions or ECMs appear. The analytical estimate of the ECM limit points use the expressions derived in Section III, now evaluated with the new values of T and θ .

VI. DISCUSSION

We have shown analytically that the pulsating intensity solution branches investigated in Ref. [29], and called ECMs, belong to isolated branches of periodic solutions. The intensity exhibits π/ω -periodic oscillations where ω is close to a multiple of $\pi\theta^{-1}$. All the solution branches were obtained by investigating the leading order solvability conditions which were relatively easy to derive. The approximations of the Hopf points and the branches of ECMs were shown to be in very good agreement with the values found by a numerical bifurcation study for realistic laser parameters.

We have found degenerate Hopf bifurcation points that result from the interaction between pulsating intensity and steady state branches. We did not find the branching to nonsymmetric periodic solutions that were noted numerically. A higher order analysis is necessary in order to unfold these degeneracies and determine other bifurcations, but this analysis is outside the scope of this paper.

Our asymptotic theory is sufficiently simple so that complications of the PCF equations can be considered, such as detuning between the frequencies of the reflected and incident waves. The linear stability analysis of the ECM solutions is also possible but again requires a higher order analysis. Physically, the leading approximation (25) of the field describes the ECM regimes as the sum of two oscillatory modes satisfying a resonance condition. A beating phenomenon between these oscillatory modes is inevitable and leads to rapidly pulsating intensity regimes exhibiting frequencies close to multiples of the external cavity frequency.

APPENDIX A: DIMENSIONLESS PCF EQUATIONS

Assuming no nonlinear gain saturation and setting the phase-shift $\phi_{\text{PCM}} = 0$, the laser rate equations introduced in Ref. [32] can be written as

$$\frac{dE}{dt'} = \frac{1}{2} [(G_N(N - N_0) - \tau_p^{-1})(1 + i\alpha)] E + \kappa E^*(t' - \tau), \quad (\text{A1})$$

$$\frac{dN}{dt'} = \frac{I}{q} - \frac{N}{\tau_e} - G_N(N - N_0) |E|^2. \quad (\text{A2})$$

Introducing the new variables t , Y and Z defined by

$$t \equiv t'/\tau_p, \quad Y \equiv \sqrt{\frac{\tau_e G_N}{2}} E \quad \text{and} \quad Z \equiv \frac{G_N \tau_p}{2} (N - N_{\text{sol}}) \quad (\text{A3})$$

into (A1) and (A2), we obtain

$$\begin{aligned} \frac{dY}{dt} &= (1 + i\alpha)YZ + \gamma Y^*(t - \theta), \\ T \frac{dZ}{dt} &= P - Z - (1 + 2Z)|Y|^2 \end{aligned} \quad (\text{A4})$$

where

$$\gamma = \kappa \tau_p, \quad \theta = \tau/\tau_p, \quad T = \tau_e \tau_p^{-1} \quad (\text{A5})$$

$$I_{th} = \frac{N_{\text{sol}} q}{\tau_e}, \quad P = \frac{G_N \tau_p \tau_e}{2} \left(\frac{I - I_{th}}{q} \right). \quad (\text{A6})$$

APPENDIX B: BASIC STEADY STATE AND HOPF BIFURCATION CONDITIONS

Introducing the decomposition

$$Y = R \exp(i\phi) \quad (\text{B1})$$

into (1) and (2), we obtain

$$R' = ZR + \gamma R(t - \theta) \cos(\phi + \phi(t - \theta)), \quad (\text{B2})$$

$$\phi' = \alpha Z - \gamma \frac{R(t - \theta)}{R} \sin(\phi + \phi(t - \theta)), \quad (\text{B3})$$

$$TZ' = P - Z - (1 + 2Z)R^2. \quad (\text{B4})$$

The steady state solution satisfies the conditions $R' = \phi' = Z' = 0$. From the steady state equations, we find two branches of solutions for Z given by

$$2\phi = -\arctan(\alpha), \quad Z = C = -\frac{\gamma}{\sqrt{1 + \alpha^2}}, \quad (\text{B5})$$

$$2\phi = \pi - \arctan(\alpha), \quad Z = C = \frac{\gamma}{\sqrt{1 + \alpha^2}} \quad (\text{B6})$$

where

$$R^2 = \frac{P - C}{1 + 2C} > 0. \quad (\text{B7})$$

Since there exist two branches of steady states for Z differing by the sign of C , it is mathematically more convenient to use C as our bifurcation parameter. From the linearized equations, we determine the characteristic equation for the growth rate λ of a small perturbation. A Hopf bifurcation is possible if λ is purely imaginary. Introducing $\lambda = i\sigma$ into the characteristic equation, we obtain from the real and imaginary parts two equations for C and σ given by

$$\begin{aligned} 0 &= \sigma [(1 + \alpha^2)C^2(\cos(2\sigma\theta) - 1) + \sigma^2] \\ &+ \varepsilon \frac{1 + 2P}{1 + 2C} [-(1 + \alpha^2)C^2 \sin(2\sigma\theta) + 2\sigma C] \\ &+ 2\varepsilon(P - C) [-(1 + \alpha^2)C \sin(\sigma\theta) - \sigma], \end{aligned} \quad (\text{B8})$$

$$\begin{aligned}
0 = & \sigma [(1 + \alpha^2)C^2 \sin(2\sigma\theta) - 2\sigma C] \\
& + \varepsilon \frac{1 + 2P}{1 + 2C} [(1 + \alpha^2)C^2 (\cos(2\sigma\theta) - 1) + \sigma^2] \\
& + 2\varepsilon(P - C)(1 + \alpha^2)C(\cos(\sigma\theta) + 1) \quad (\text{B9})
\end{aligned}$$

where ε is defined by (4).

ACKNOWLEDGMENTS

The research of TE and AG was supported by the US Air Force Office of Scientific Research grant

AFOSR F49620-98-1-0400, the National Science Foundation grant DMS-9973203, the Fonds National de la Recherche Scientifique (Belgium) and the InterUniversity Attraction Pole program of the Belgian government. KG is a Research Fellow of the Katholieke Universiteit Leuven (Belgium). The research of BK is supported by an EPSRC Advanced Research Fellowship grant.

-
- [1] C. O. Weiss and R. Vilaseca, Dynamics of Lasers, VCH Weinheim, FRG (1991)
 - [2] D. Lenstra (Ed), Fundamental Nonlinear Dynamics of Semiconductor Lasers, Quantum and Semiclass. Optics 9 (1997)
 - [3] G. H. M. Van Tartwijk and G. P. Agrawal, Laser instabilities: a modern perspective. *Prog. Quantum Electron.*, 22:43 (1998)
 - [4] B. Krauskopf and D. Lenstra (Eds), Fundamental Issues of Nonlinear Laser Dynamics, AIP Conference Proceedings 548 (2000)
 - [5] E. Lacot, R. Day and F. Stoeckel, Coherent laser detection by frequency-shifted optical feedback, *Phys. Rev. A* **64**, 043815 (2001)
 - [6] E. Lacot, R. Day, J. Pinel, and F. Stoeckel, Laser relaxation-oscillation frequency imaging, *Optics Letters* **26**, 1483 (2001)
 - [7] J. Mørk, J. Mark and B. Tromborg, Route to chaos and competition between relaxation oscillations for a semiconductor laser with optical feedback, *Phys. Rev. Lett.* **65**, 1999-2002 (1990)
 - [8] J. Mørk, B. Tromborg, and J. Mark, Chaos in semiconductor lasers with optical feedback: theory and experiment, *IEEE J. Quantum Electron.* **28**, 93-108 (1992)
 - [9] Y. Cho and T. Umeda, Observation of chaos in semiconductor lasers with delayed feedback, *Opt. Comm.* **59**, 131-136 (1986)
 - [10] D. Lenstra, B. H. Verbeek, and J. den Boef, Coherence collapse in single-mode semiconductor lasers due to optical feedback, *IEEE J. Quantum Electron.* **21**, 674-679 (1985)
 - [11] H. Li, J. Ye, and J. G. McInerney, Detailed analysis of coherence collapse in semiconductor lasers, *IEEE J. Quant. Electron.* **29**, 2421-2432 (1993)
 - [12] G. H. M. Van Tartwijk and D. Lenstra, Semiconductor lasers with optical injection and feedback, *Quant. Semiclass. Opt.* **7**, 87-143 (1995)
 - [13] G. H. M. Van Tartwijk, A. M. Levine and D. Lenstra, Sisyphus effect in semiconductor lasers with optical feedback, *IEEE J. of Select. Top. in Quant. Electronics* **1**, 466-472 (1995)
 - [14] G. H. M. Van Tartwijk, H. J. C. van der Linden, and D. Lenstra, Theory of a diode laser with phase-conjugate feedback, *Opt. Letters* **17**, 1590-1592 (1992)
 - [15] G. R. Gray, D. Huang, and G. P. Agrawal, Chaotic dynamics of semiconductor lasers with phase-conjugate feedback, *Phys. Rev. A* **49**, 2096-2105 (1994)
 - [16] C. R. Giuliano, Applications of optical phase conjugation. *Physics Today*, 34(4):27-35 (April 1981)
 - [17] D. H. DeTienne, G. R. Gray, G. P. Agrawal, and D. Lenstra, Semiconductor laser dynamics for feedback from a finite-penetration-depth phase-conjugate mirror, *IEEE J. of Quantum Electronics* **33**, 838-844 (1997)
 - [18] W. A. van der Graaf, L. Pesquera, and D. Lenstra, Stability properties of diode lasers with phase-conjugate feedback, In *Physics and Simulations of Optoelectronic Devices VI*, W. W. Chow, M. Osinski, Eds., SPIE Proc. **3283**, 522-533 (1998)
 - [19] W. A. van der Graaf, L. Pesquera, and D. Lenstra, Stability of a diode laser with phase-conjugate feedback, *Opt. Letters* **23**, 256-258 (1998)
 - [20] B. Krauskopf, G. R. Gray, and D. Lenstra, Bifurcation in a semiconductor laser with phase-conjugate feedback, in *Physics and Simulations of Optoelectronic Devices VI*, W. W. Chow, M. Osinski, Eds., SPIE Proc. **3283**, 510-521 (1998)
 - [21] B. Krauskopf, G. R. Gray, and D. Lenstra, Semiconductor laser with phase-conjugate feedback: dynamics and bifurcations, *Phys. Rev. E* **58**, 7190-7197 (1998)
 - [22] A. Murakami, J. Ohtsubo and Y. Liu, Stability analysis of semiconductor laser with phase-conjugate feedback, *IEEE J. of Quantum Electronics* **33**, 1825-1831 (1997)
 - [23] K. Engelborghs, T. Luzyanina, and G. Samaey, DDE-BIFTOOL v2.00: a Matlab package for bifurcation analysis of delay differential equations. Technical Report TW-330, Department of Computer Science, K. U. Leuven, Belgium, 2002. <http://www.cs.kuleuven.ac.be/~koen/delay/ddebiftool.shtml>
 - [24] D. Pieroux, T. Erneux, B. Haegeman, K. Engelborghs and D. Roose, Bridges of periodic solutions and tori in semiconductor lasers subject to delay, *Phys. Rev. Lett.* **87**, 193901 (2001)
 - [25] M. Sciamanna, T. Erneux, F. Rogister, O. Deparis, P. Mégret, and M. Blondel, Bifurcation bridges between external-cavity modes lead to polarization self-modulation in vertical-cavity surface-emitting lasers, *Phys. Rev. A* **65**, 041801(R) (2002)
 - [26] M. Sciamanna, F. Rogister, O. Deparis, P. Mégret, M. Blondel, and T. Erneux, Bifurcation to polarization self-modulation in vertical-cavity surface-emitting lasers, *Opt. Lett.* **24**, 261-263 (2002)
 - [27] B. Haegeman, K. Engelborghs, D. Roose, D. Pieroux and

- T. Erneux, Stability and rupture of bifurcation bridges in semiconductor lasers subject to optical feedback, *Phys. Rev. E* **66**, 046216 (2002)
- [28] T. Erneux, A. Gavrielides and M. Sciamanna, Stable microwave oscillations due to external-cavity-mode beating in laser diodes subject to optical feedback, *Phys. Rev. A* **66**, 033809 (2002)
- [29] K. Green and B. Krauskopf, Bifurcation analysis of frequency locking in a semiconductor laser with phase-conjugate feedback, *International Journal of Bifurcation and Chaos*, to appear (2003); available as a preprint at <http://www.enm.bris.ac.uk/anm/preprints/2002r06.html>
- [30] T. Erneux, F. Rogister, A. Gavrielides, and V. Kovanis, Bifurcation to mixed external cavity mode solutions for semiconductor lasers subject to optical feedback, *Opt. Comm.* **183**, 467-477 (2000)
- [31] A. Gavrielides, Nonlinear dynamics of semiconductor lasers: Theory and experiments, In Krauskopf and Lenstra [4], pages 191–217.
- [32] K. Green and B. Krauskopf, Global bifurcations and bistability at the locking boundaries of a semiconductor laser with phase-conjugate feedback, *Phys. Rev. E* **66**, 016220 (2002)
- [33] K. Green, B. Krauskopf, and K. Engelborghs, Bistability and torus break-up in a semiconductor laser with phase-conjugate feedback, *Phys. D* **173**, 114–129 (2002)
- [34] K. Green, B. Krauskopf, and G. Samaey, A two-parameter study of the locking region of a semiconductor laser subject to phase-conjugate feedback, *SIAM J. Applied Dynamical Systems* **2**, 254-276 (2003)
- [35] B. Krauskopf, G. H. M. Van Tartwijk, and G. R. Gray, Symmetry properties of lasers subject to optical feedback, *Opt. Comm.* **177**, 347 (2000)
- [36] C. M. Bender and S. A. Orszag, *Advanced Mathematical Methods for Scientists and Engineers*, Mc Graw Hill, New York (1978)
- [37] J. Kevorkian and J. D. Cole, *Perturbation Methods in Applied Mathematics*, Applied Mathematical Sciences 34, Springer, New York (1981); *Multiple Scale and Singular Perturbation Methods*, Applied Mathematical Sciences 114, Springer, New York (1996)
- [38] T. Erneux, Asymptotic methods applied to semiconductor laser models, in *Physics and Simulations of Optoelectronic Devices VIII*, R. Binder, P. Blood, M. Osinski, Eds., *Proc. SPIE* 3944, 588-601 (2000)